

Effects of welding current on properties of A-TIG welded AZ31 magnesium alloy joints with TiO₂ coating

Jun SHEN, Da-jun ZHAI, Kai LIU, Zhong-ming CAO

College of Materials Science and Engineering, Chongqing University, Chongqing 400044, China

Received 24 July 2013; accepted 5 November 2013

Abstract: The effects of welding current on the macro-morphology, microstructure and mechanical properties of tungsten inert gas (TIG) welded AZ31 magnesium alloy joints with TiO₂ coating were investigated. The results showed that the increase of welding current led to the increase in the depth/width ratio and deteriorated the surface appearance of the welded seams with TiO₂ coating. The grain size of α -Mg and the amount of granular β -Mg₁₇Al₁₂ particles in the welded seams also increased. The welded joints with TiO₂ coating exhibited a deeper weld penetration and larger grain size compared with the welded joint without TiO₂ coating. When the welding current was less than 130 A, the ultimate tensile strength of the welded joints with TiO₂ coating increased with the increase in welding current and then decreased when the welding current was greater than 130 A. The average microhardness of the heat-affected zone and fusion zone decreased gradually with the increase of welding current.

Key words: AZ31 magnesium alloy; A-TIG welding; welding current; TiO₂ coating

1 Introduction

TIG welding technology is adopted widely for magnesium alloys because of its advantages of economy and utility, whereas the relatively shallow penetration in single pass welding and low productivity restrict the application of TIG welding on magnesium alloys [1].

For improving the TIG welding quality of magnesium alloys, an activating flux tungsten inert gas (A-TIG) welding technology has been developed. This technology is characterized by the application of a fine layer of an activating flux on the top surface of the base material (BM) before TIG welding to get a greatly increased weld penetration [2]. Some researchers considered that the increase of the weld penetration was caused by the constriction of the electric arc [3]. Others believed that the greater penetration was due to the change in the liquid flow of molten metal in weld pool [4,5]. LIU et al [6,7] studied the mechanism and microstructure of oxide fluxes for gas tungsten arc welding of magnesium alloy. They found that five single oxide fluxes, MgO, CaO, TiO₂, MnO₂ and Cr₂O₃, increased the weld penetration effectively because the

oxide fluxes affected the liquid flow of molten metal in the weld pool. WANG et al [8] studied the effects of TiO₂ coating on the microstructure and mechanical properties of tungsten inert gas welded AZ31 magnesium alloy joints. They reported that with the increase of the amount of TiO₂ coating, the weld penetration increased significantly and the mechanical properties also improved. Too much TiO₂ coating led to the coarsening of the grains in the welded seam and then resulted in poor mechanical properties of the welded joints.

Above investigations reported the mechanisms of the deep weld penetration of the A-TIG welded magnesium alloy joints and the effects of the amount of flux on the microstructure and mechanical properties of the welded magnesium alloy joints. Relatively few investigations have been carried out to determine the influences of welding parameters (especially welding current) on the microstructure and mechanical properties of the welded magnesium alloy joints with flux coating. In addition, welding current is extremely sensitive to the welding process, especially the thickness of welding joints, the width of welding seams and the species of activating flux. Therefore, in this work, the effects of welding current on the microstructure and mechanical

properties of TIG welded magnesium alloy joints with TiO₂ coating are investigated in detail.

2 Experimental

Hot-extruded AZ31 magnesium alloy plates (the average composition (mass fraction): 3.27% Al, 0.91% Zn, 0.25% Mn, <0.10% Si, <0.05% Cu, <0.04% Ca, <0.005% Fe, <0.005% Ni, balance Mg) with a dimension of 100 mm×50 mm×6 mm were used for the welding tests. AC automatic welding machine (NSA-500-1) with an arc voltage control (HAS-01-A) was applied for butt-welding tests, and the experimental trials were butted in a mechanical jig by depositing the trials on low-carbon steel bars. The gap width of the trials was about 0.1 mm. The welding current of different specimens was 110 A, 120 A, 130 A (without TiO₂ coating), 130 A (with TiO₂ coating), 140 A, 150 A, respectively. The other welding parameters were as follows: welding voltage of (15±0.3) V, welding speed of 300 mm/min and flow rate of shielding gas (argon) of 15 L/min. In order to ensure the accuracy and comparability of the trials, the electrodes were ground into standard shape before welding and the arc was adjusted to standard length to guarantee the united standard of welding.

Before welding, the surface of each specimen was ground using a grinder to remove oxides and then they were cleaned with acetone to eliminate surface contamination. The TiO₂ with particle size of about 120 nm was selected as activating flux and mixed with acetone. Then the mixture was applied to the top surface of specimens with a width of about 40 mm. The mass of plates before coating (m_1) and the mass of plates after coating (m_2) were weighed with an electrical analytical balance (with accuracy of 0.1 mg). Then, the amount of the flux coating on the unit area of different specimens (ρ_A) was calculated by the formula as follows:

$$\rho_A = \frac{m_1 - m_2}{S} \quad (1)$$

where S is the coated area. The amount of the flux coating on the unit area was constant (about (5±0.2) mg/cm²).

After welding, the cross-sections of the welded seams were prepared by standard metallographic procedures, including grinding, polishing and etching (with the solution containing 5 g picric acid + 90 mL ethyl alcohol + 5 mL acetic acid + 10 mL distilled water). Three different cross-sections in the middle of each welded joint were prepared for measuring the weld dimension. The microstructure of the welded joints was observed by an optical microscope (MDJ200). Based on the quantitative stereology theory defined by XU and CHEN [9], the average grain size (d) of the primary

phase in the welded seams was evaluated by the formula as follows:

$$V_V = A_A = L_L, \quad d = L \cdot L_L / N_L \quad (2)$$

where V_V is the volume fraction of the primary phase, A_A is the area percentage of the primary phase in a cross-section of the welded seam, L_L is the ratio of the random line segments through the primary phase to the length of total line in the cross-section, L is the length of measuring line, N_L is the number of grains on the line.

An energy dispersive X-ray spectroscopy (OXFORD, Inc., ISIS300, EDS) was used for detecting the distribution of elements in the welded seams. The fracture surfaces of the welded joints and the BM were observed by a scanning electron microscope (TESCAN VEGA II LMV, SEM). The tensile tests were carried out by an electronic testing machine (SANS XYA105C) at room temperature with a rate of 0.3 mm/min and the tensile direction was perpendicular to the welded seams. Three tensile test results were collected on samples with the same welding current and the average values of them were adopted. The microhardness tests were performed across the weld cross-section by a Vickers hardness tester (HX-1000TM). The values of microhardness of the HAZ and fusion zone (FZ) were obtained from an average value of five data points.

3 Results and discussion

3.1 Macro-morphologies of welded seams

The surface appearances and the outlines of FZ of the TIG welded seams under different welding currents are shown in Figs. 1 and 2, respectively. The effects of welding current on the depth/width (D/W) ratio and the average width of the welded seams are shown in Fig. 3. With the increase of welding current, the surfaces of the welded seams with TiO₂ coating became irregular and even there appeared serious collapse on the surface of the welded seam when too high welding current was adopted (Fig. 1). The weld penetration of the welded seams with TiO₂ coating increased gradually with the increase of welding current and a full-penetration occurred at current of 130 A (Fig. 2). The TiO₂ coating led to significant increases in the weld penetration capability, up to 150% compared with the normal welded seam without flux at the same welding current (Figs. 2(c) and (d)). The width of the welded seams with TiO₂ coating increased obviously when relatively low welding currents were adopted, whereas the width of the welded seams changed slightly (Fig. 3) under higher welding current. The D/W ratio increased with the increase of welding current when relatively low welding current was adopted. When the welding current arrived to 130 A, the D/W ratio of the welded seams began to decrease gradually with the

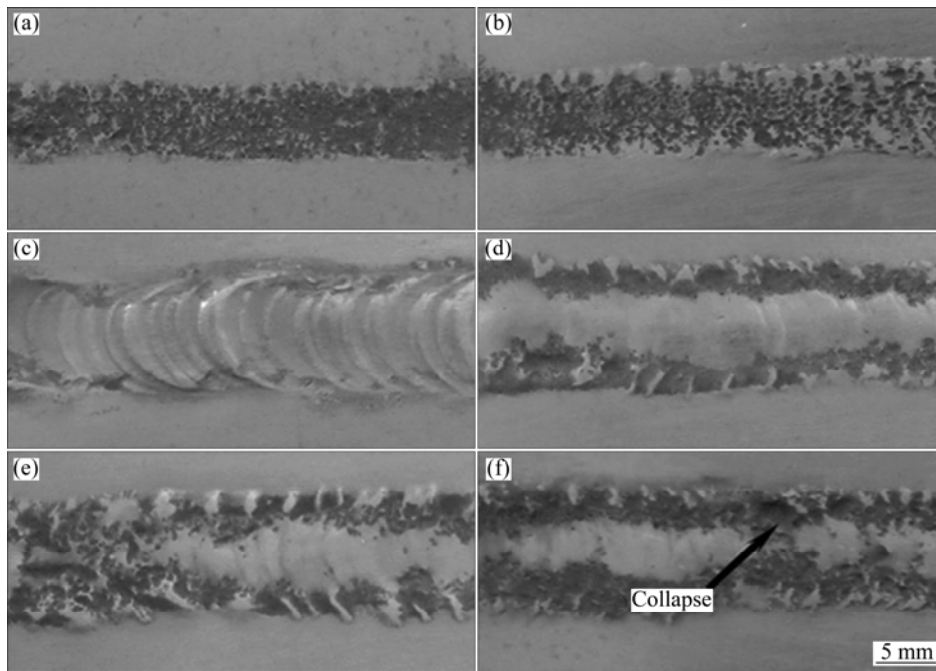


Fig. 1 Appearances of TIG welded seams under different welding currents: (a) 110 A with TiO_2 coating; (b) 120 A with TiO_2 coating; (c) 130 A without TiO_2 coating; (d) 130 A with TiO_2 coating; (e) 140 A with TiO_2 coating; (f) 150 A with TiO_2 coating

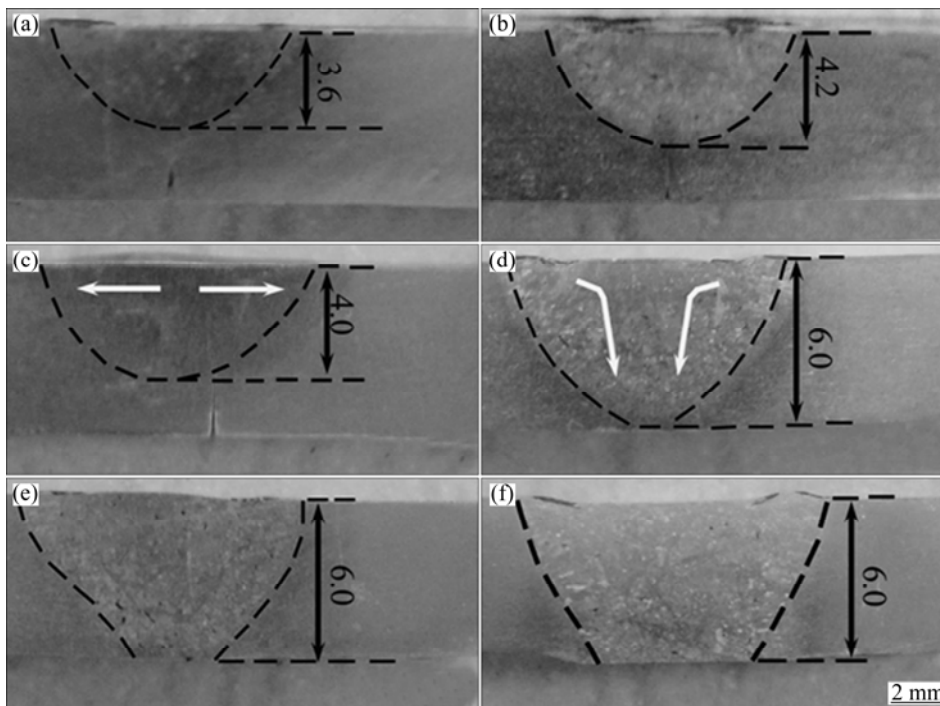


Fig. 2 Cross-sections of TIG welded seams under different welding currents: (a) 110 A with TiO_2 coating; (b) 120 A with TiO_2 coating; (c) 130 A without TiO_2 coating; (d) 130 A with TiO_2 coating; (e) 140 A with TiO_2 coating; (f) 150 A with TiO_2 coating

increase of welding current (Fig. 3).

The high welding current led to a large heat input of the weld pool [10], which in turn increased the weld penetration and the width of the welded seams. Previous researches [11,12] showed that the shape of the welded seam was determined by the change of the liquid flow in the weld pool. For the sample that was welded without

TiO_2 coating, the temperature coefficient of surface tension of the weld pool was a negative value. Under this condition, the fluid flow of the molten pool surface transferred easily from the pool center to the edge, resulting in the formation of a wide and shallow welded seam (Fig. 1(c) and Fig. 2(c)). On the contrary, when TiO_2 coating was adopted, the temperature coefficient of

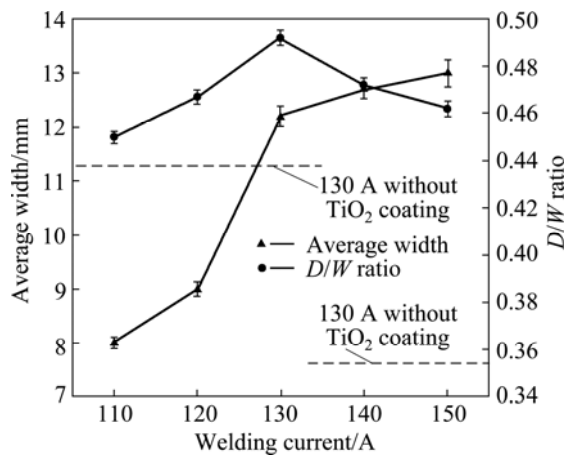


Fig. 3 Effects of welding current on depth/width ratio (D/W) and average width of welded seams

surface tension on the molten pool changed from a negative to a positive value. In this situation, the fluid flow of the molten pool surface transferred from the pool

edge to the center easily, leading to the formation of narrow and deep welded seams (Fig. 1(d) and Fig. 2(d)).

The distribution of elements in the FZ of the TIG welded seams with and without TiO_2 coating was measured by EDS analysis. The regions measured included the top, bottom and middle of the FZ. The EDS results of the welded seams with and without TiO_2 coating at the same welding current are shown in Fig. 4. The remaining non-metallic element (oxygen) is not shown in Fig. 4. The content of Al and Zn elements in the welded seam with TiO_2 coating (Fig. 4(b)) was lower than that without TiO_2 coating (Fig. 4(a)). This proved that the evaporation of the Al and Zn elements was promoted by the TiO_2 coating. With the increase of welding current, the evaporation of Zn and Al elements was increased. Hence, the surfaces of the welded seams with TiO_2 coating were deteriorated under high welding current condition. In addition, Ti element was distributed both in the middle and bottom of the FZ of the welded seams with TiO_2 coating (as seen in Fig. 4(b)). This

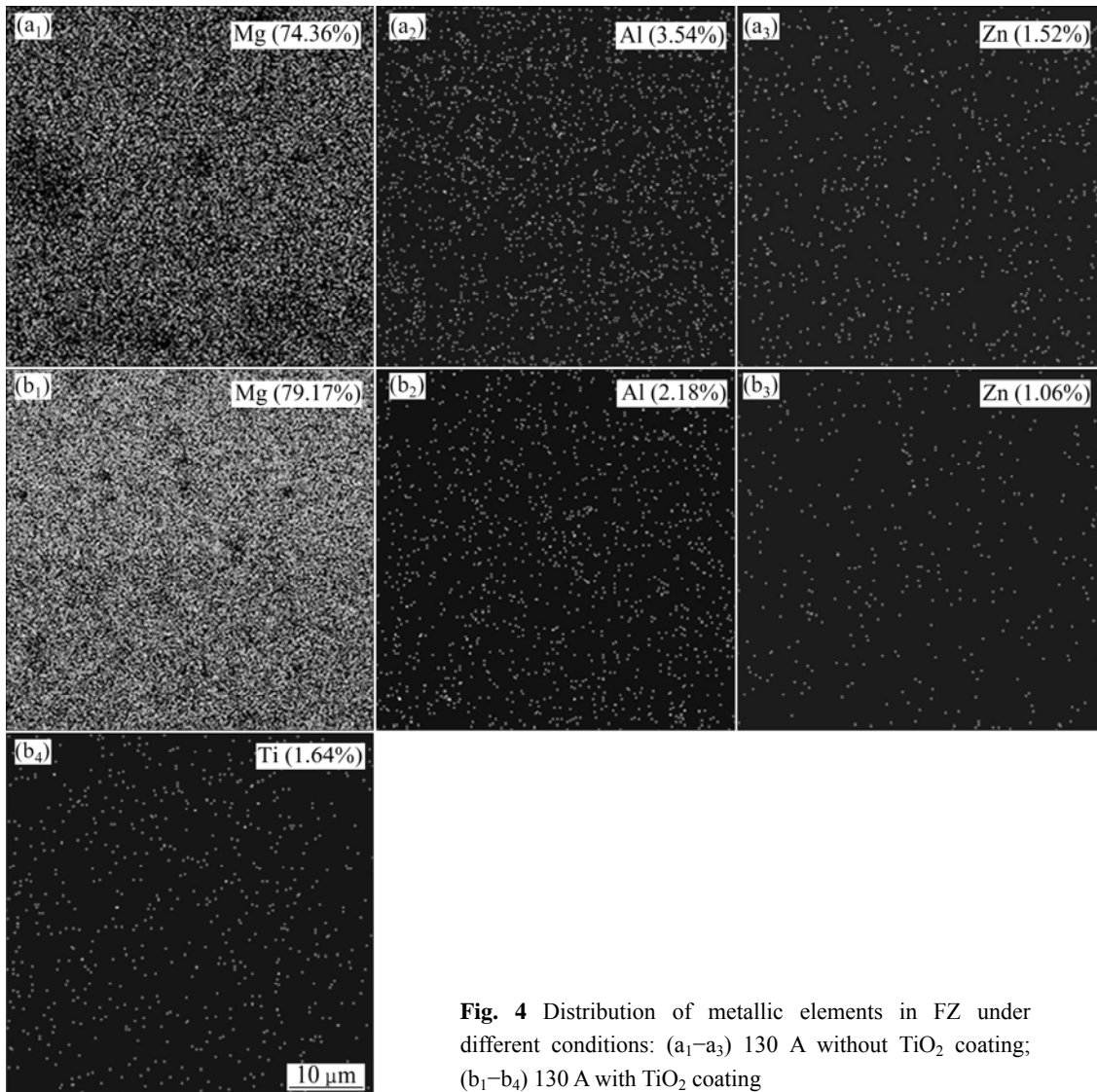


Fig. 4 Distribution of metallic elements in FZ under different conditions: (a₁–a₃) 130 A without TiO_2 coating; (b₁–b₄) 130 A with TiO_2 coating

proved that the greater penetration was caused by the change of the liquid flow in the weld pool.

3.2 Microstructures of welded seams

3.2.1 Typical microstructure of TIG welded AZ31 magnesium alloy joints with TiO₂ coating

Figure 5 shows a typical microstructure of the TIG welded AZ31 magnesium alloy joints with TiO₂ coating. The welded joint consists of BM, fusion zone (FZ) and heat-affected zone (HAZ). The microstructure of the BM is characterized by non-uniform equiaxed grains formed by the recrystallization during the hot extrusion process. According to ZHANG et al's results [13,14] and the Mg–Al binary phase diagram, the FZ and HAZ are mainly composed of primary-phase (α -Mg) (marked with arrow *A* in Fig. 5) and second-phase (β -Mg₁₇Al₁₂) (marked with arrow *B* in Fig. 5).

3.2.2 Effects of welding current on microstructure of HAZ

Figure 6 illustrates the evolution of microstructure of the HAZ in the welded joints with the increase of welding current. The average grain size (*d*) of the α -Mg

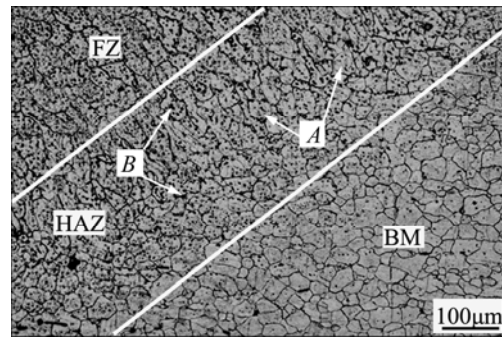


Fig. 5 Typical microstructural image of TIG welded AZ31 magnesium alloy joint with TiO₂ coating

grains in the HAZ under different welding currents is listed in Table 1. With the increase of welding current, the width of the HAZ was increased due to the extra heat input to the BM and the grain size of α -Mg grains in the HAZ was also increased (Fig. 6). The width of the HAZ of the welded joint with TiO₂ coating was wider and the average size (*d*) of α -Mg grains (57 μ m) in the HAZ was larger than those without TiO₂ coating (Figs. 6(c) and (d)).

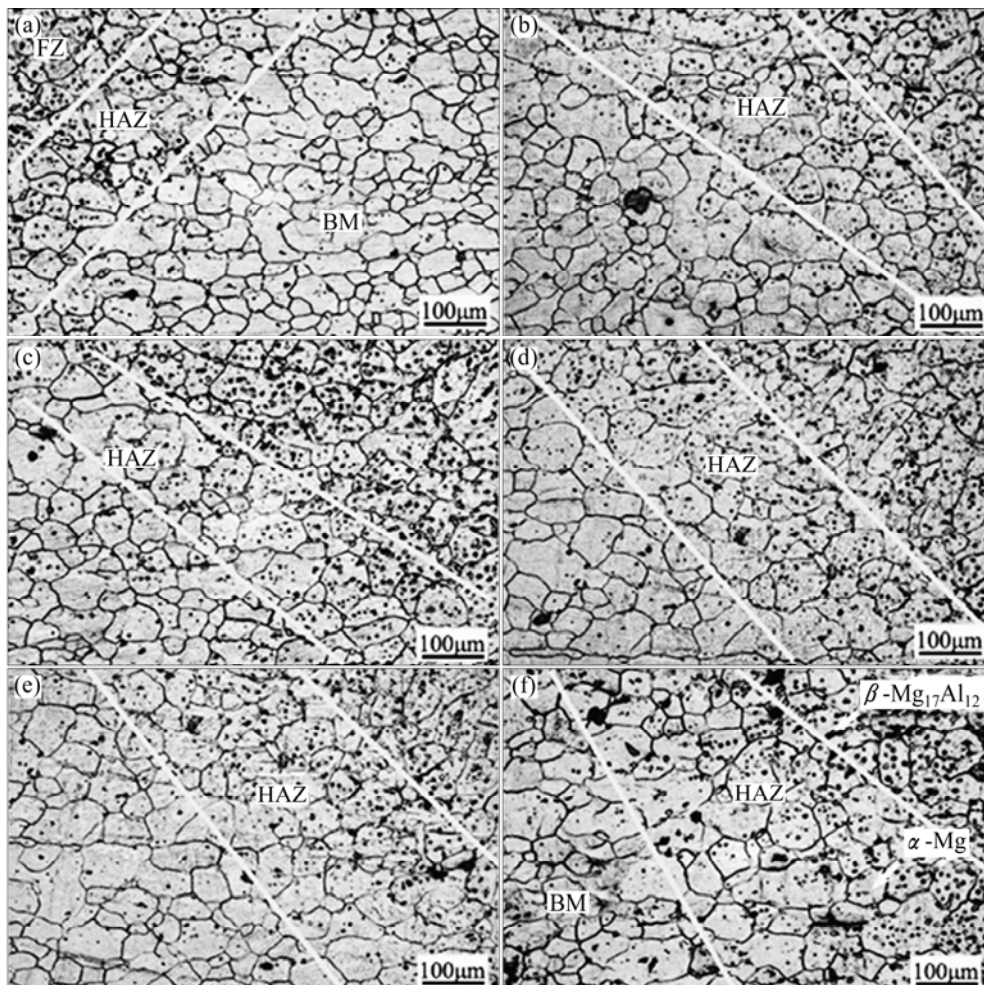


Fig. 6 Microstructures of TIG welded joints under different welding currents: (a) 110 A with TiO₂ coating; (b) 120 A with TiO₂ coating; (c) 130 A without TiO₂ coating; (d) 130 A with TiO₂ coating; (e) 140 A with TiO₂ coating; (f) 150 A with TiO₂ coating

Table 1 Average grain size (d) of α -Mg grains in HAZ under different welding currents

Welding current/A	TiO ₂ coating	$d/\mu\text{m}$
110	With	49±0.8
120	With	52±1.1
130	Without	50±0.9
130	With	57±1.5
140	With	64±1.3
150	With	73±1.8

The temperature in the HAZ may be up to 527 K during the welding process [15], which is higher than the recrystallization temperature of the AZ31 magnesium alloys (about 478 K) [16]. Therefore, recrystallization and grain coarsening occur in the HAZ and higher welding current leads to a longer recrystallization time. Moreover, when the welded seams are covered by TiO₂ coating, since the temperature at the boundary of the welding pool is below the liquidus of TiO₂, part of the

TiO₂ coating does not melt in the welding pool and then reduces the velocity of liquid flow from the pool center to the edge in the welding pool. The heat transported by conduction increases, resulting in the increase of the width of the HAZ of the welded joints slightly.

3.2.3 Effects of welding current on microstructure of FZ

The effects of welding current on the microstructure of the FZ of the welded AZ31 magnesium alloy joints are shown in Fig. 7. The average size (d) of α -Mg grains in the FZ is shown in Table 2. The α -Mg grains in the FZ coarsened gradually with the increase of welding current (Fig. 7). When the welding current increased to the maximum value (150 A), the average grain size arrived to 62 μm (Table 2). The average size (d) of the α -Mg grains with TiO₂ coating (48 μm) in the FZ is larger than that without TiO₂ coating (44 μm) (Figs. 7(c) and (d)). This is because the increase of heat input and the low heat loss promote the growth of α -Mg grains. By careful observation (Figs. 7(a)–(b) and (d)–(f)), the amount of granular β -Mg₁₇Al₁₂ particles in the FZ increased with the increase of welding current.

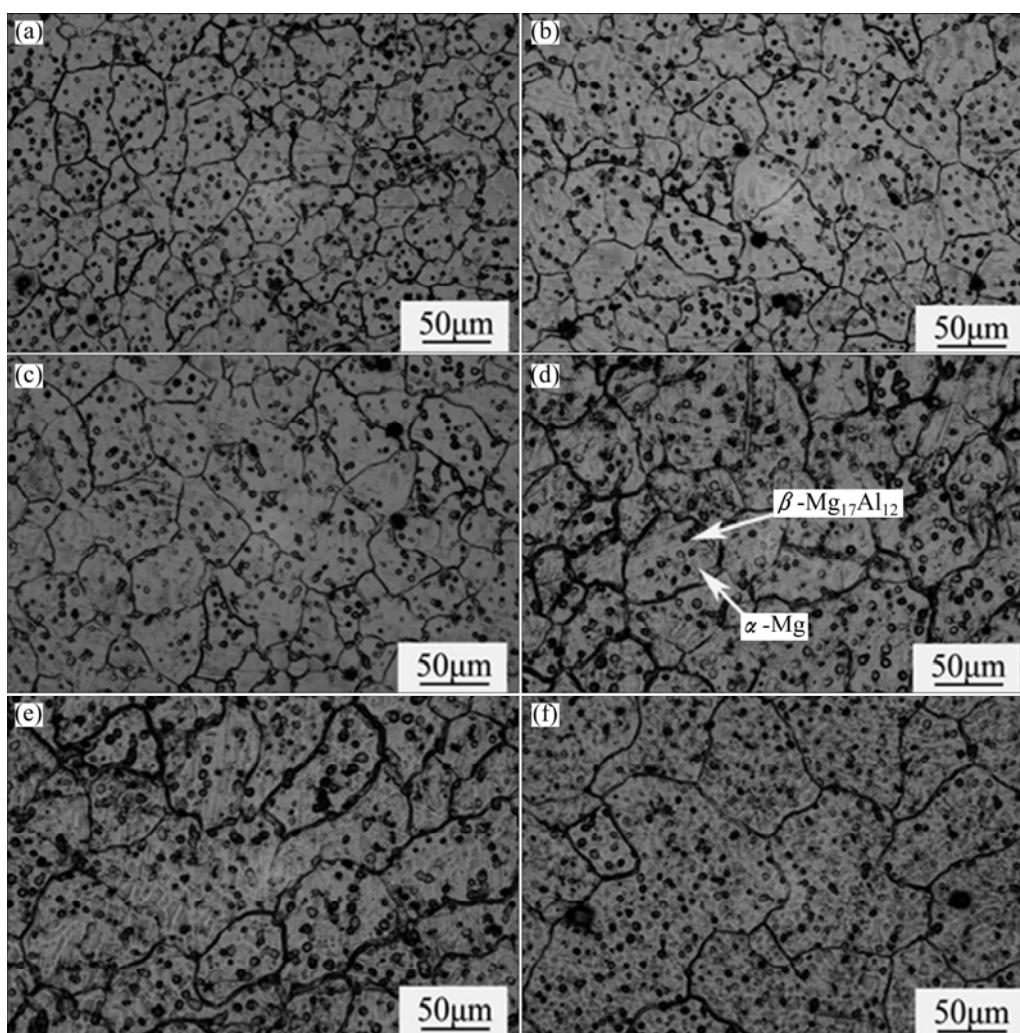


Fig. 7 Microstructures of FZ of TIG welded joints under different welding currents: (a) 110 A with TiO₂ coating; (b) 120 A with TiO₂ coating; (c) 130 A without TiO₂ coating; (d) 130 A with TiO₂ coating; (e) 140 A with TiO₂ coating; (f) 150 A with TiO₂ coating

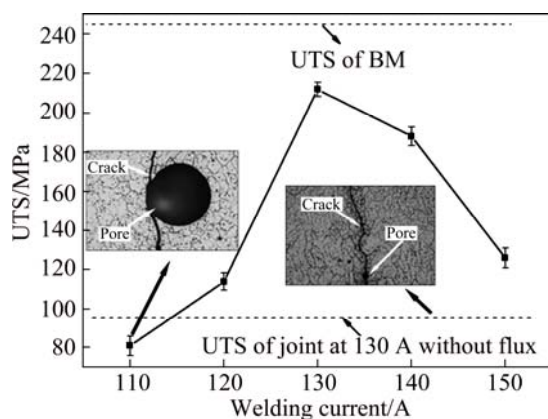
Table 2 Average grain size (d) of α -Mg grains in FZ under different welding currents

Welding current/A	TiO ₂ coating	$d/\mu\text{m}$
110	With	40±0.4
120	With	43±0.4
130	Without	44±1.1
130	With	48±0.7
140	With	54±1.3
150	With	62±0.9

3.3 Mechanical properties of welded seams

3.3.1 Tensile strength

The effect of welding current on the ultimate tensile strength (UTS) of the TIG welded joints is depicted in Fig. 8. A partial penetration (Fig. 2(a)) appeared in the welded seam at current of 110 A with TiO₂ coating. Under this condition, the UTS value of the welded joint was 81 MPa, which was only 33% of that of the BM (245 MPa). With the increase of welding current, the UTS value of the welded joints with TiO₂ coating increased gradually. The highest UTS value (212 MPa) of the welded joints, 86% of that of the BM, was obtained when the welding current was 130 A. Whereas when the welding current was over 130 A, the UTS value of the welded joints began to decrease. For example, the UTS value of the welded joints decreased greatly when the welding current was 150 A, which was only 51% of that of the BM. The UTS value of the welded joint without TiO₂ coating welded at 130 A was 95 MPa, which was only 45% of that of the welded joint with TiO₂ coating at the same welding current for the pores and cracks (Fig. 8) formed in the welded joint.

**Fig. 8** Effect of welding current on UTS of TIG welded AZ31 magnesium alloy joints

During the welding process, the surface of the molten pool was protected by the shielding gas, while the back of the sample failed to be protected. Hence, air intruded into the weld pool easily through the gap between the two plates. The molten pool was solidified

so quickly that the air had no enough time to escape from the molten pool when the welding current was too low, resulting in the formation of the pores in the welded joint and cracks formed along the pores due to the concentration of the welding stress (Fig. 8). Therefore, the mechanical strength of the welded joint was weakened largely. With the increase of the welding current, the relatively low cooling rate avoided the rapid solidification of the molten pool and the air had enough time to escape from the weld pool and then the porosity decreased. Hence, the mechanical strength of the welded joint improved gradually. Too high welding current caused the serious coarsening of α -Mg grains in the HAZ (Fig. 6(f)). Moreover, there appeared serious collapse on the surface of the welded seam (Fig. 1(f)). All of those led to the decrease of the mechanical strength of the welded joint sharply.

The tensile fracture surfaces of the BM and the welded joints with TiO₂ coating are shown in Fig. 9. The fractures of the welded joints occurred in the FZ when the welding current was below 130 A. However, when the welding current was above 130 A (including 130 A), the fractures of the welded joints occurred in the HAZ. The fracture surface of the BM mainly shows a feature of ductile fracture, which is characterized by more tearing fibers and ridges (Fig. 9(a)). Under low welding current, the fracture surfaces of the welded joints exhibited a character of a mixed fracture with obvious shear lips and dimples (Figs. 9(b) and (c)). Under high welding current, the fracture surface of the welded joints mainly revealed a character of cleavage fracture which belonged to a brittle fracture (Fig. 9(d)).

Too low welding current led to the segregation of the brittle β -Mg₁₇Al₁₂ particles along the grain boundaries in the FZ (as seen in Fig. 7(a)). Meanwhile, the pores and cracks formed in the FZ (Fig. 8) also caused stress concentration, which led to the fracture occurring in this zone. With the increase of welding current, the pores and cracks decreased gradually and the continuous β -Mg₁₇Al₁₂ dissolved in the FZ partially (the average size of α -Mg grain in the HAZ and the width of the HAZ increased dramatically (Figs. 6(d)–(f))). Hence, the fractures occurred in the HAZ of the welded joints.

3.3.2 Microhardness

Figure 10 shows the distribution of the microhardness of the TIG welded joint with the TiO₂ coating at current of 130 A. Compared with the BM, the microhardness of the FZ and HAZ reduced obviously. According to MERIC et al [17], an increase in the grain size leads to the decrease of the microhardness of the samples. The effect of welding current on the microhardness of the FZ and HAZ of the welded seams is shown in Fig. 11. With the increase of welding current, the microhardness of the FZ and HAZ decreased

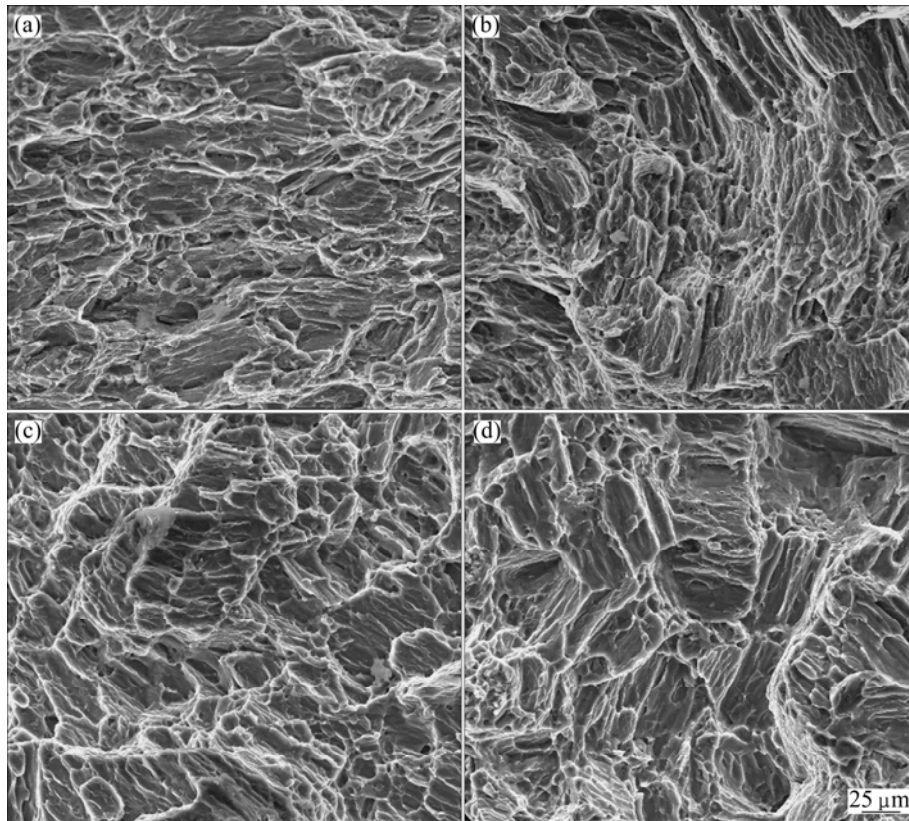


Fig. 9 Tensile fracture surfaces of BM and welded joints: (a) BM; (b) Joint welded at 110 A with TiO₂ coating; (c) Joint welded at 130 A with TiO₂ coating; (d) Joint welded at 150 A with TiO₂ coating

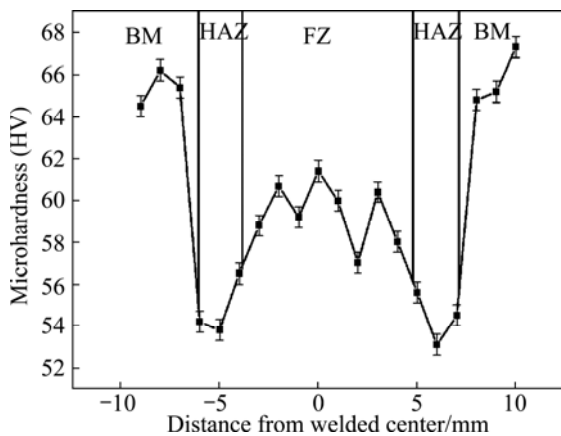


Fig. 10 Microhardness profile across welded joint at welding current of 130 A with TiO₂ coating

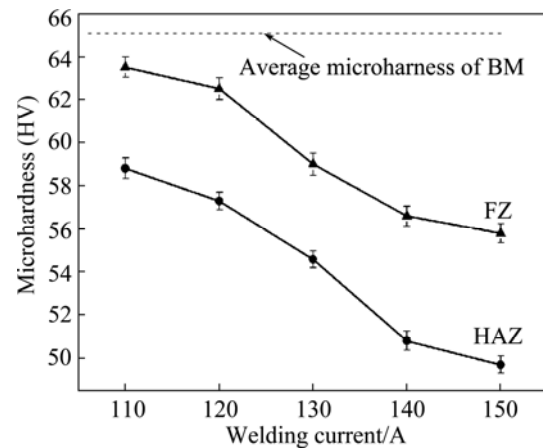


Fig. 11 Effect of welding current on microhardness of HAZ and FZ

gradually (Fig. 11). In addition, it can be seen that with the further increase of welding current, the microhardness of the FZ and HAZ changed slightly.

In general, the microhardness depends on the grain refinement and the strengthening effect of the β -Mg₁₇Al₁₂ particles [18]. When TiO₂ coating was adopted in TIG welding, the coarsening of the grains occurred both in the HAZ and FZ. Hence, the microhardness value decreased. Under high welding current, more granular β -Mg₁₇Al₁₂ particles formed in the HAZ and FZ, which

offset the effect of the grain coarsening on the decrease of microhardness of the HAZ and FZ of the welded seams partially.

4 Conclusions

1) The increase of welding current resulted in the increase of the D/W ratio and the width of the welded seam when TiO₂ coating was adopted. Too high welding current decreased the D/W ratio and deteriorated the

surface appearance of the samples.

2) When the welding current was 130 A, the TIG welded joint with TiO₂ coating exhibited a deeper weld penetration and larger grain size compared with the welded joint without TiO₂ coating, which led to relatively high UTS value of the welded joints.

3) For the welded seams with TiO₂ coating, the grain size of α -Mg and the amount of granular β -Mg₁₇Al₁₂ particles both in the FZ and HAZ increased with the increase of welding current.

4) The UTS value of the welded joints with TiO₂ coating increased firstly and then decreased with the increase in welding current when the welding current was between 110 A and 150 A, and the maximum of UTS value was 212 MPa when the welding current was 130 A.

5) For the welded seams with TiO₂ coating, the microhardness of the FZ and HAZ in AZ31 magnesium alloy welded joints decreased gradually with the increase of welding current.

References

- [1] LI Shi-zeng, SHEN Jun, CAO Zhong-ming, WANG Lin-zhi, XU Nan. Effects of mix activated fluxes coating on microstructures and mechanical properties of tungsten inert gas welded AZ31 magnesium alloy joints [J]. Science and Technology of Welding and Joining, 2012, 17(6): 467–475.
- [2] ZHANG Zhao-dong, LIU Li-ming, SHEN Yong, WANG Lai. Activating electron beam welding [J]. The Chinese Journal of Nonferrous Metals, 2005, 15(6): 912–916. (in Chinese)
- [3] HOWSE D S, LUCAS W. Investigation into arc constriction by active fluxes for tungsten inert gas welding [J]. Science and Technology of Welding and Joining, 2000, 5(3): 189–193.
- [4] YANG Chun-li, LIN San-bao, LIU Feng-yao, ZHANG Qing-tao. Research on the mechanism of penetration increase by flux in A-TIG welding [J]. Journal Materials Science and Technology, 2003, 19: 225–227.
- [5] XU Y L, DONG Z B, WEI Y H, YANG C L. Marangoni convection and weld shape variation in A-TIG welding process [J]. Theoretical and Applied Fracture Mechanics, 2007, 48(2): 178–186.
- [6] LIU L M, ZHANG Z D, SONG G, WANG L. Mechanism and microstructure of oxide fluxes for gas tungsten arc welding of magnesium alloy [J]. Metallurgical and Materials Transactions A, 2007, 38(3): 649–658.
- [7] LIU L M, ZHANG Z D, YONG S, WANG L. Effects of activating fluxes on TIG welding penetration of magnesium alloy [J]. Acta Metallurgica Sinica, 2006, 42(4): 399–404. (in Chinese)
- [8] WANG Lin-zhi, SHEN Jun, XU Nan. Effects of TiO₂ coating on the microstructures and mechanical properties of tungsten inert gas welded AZ31 magnesium alloy joints [J]. Materials Science and Engineering A, 2011, 528(24): 7276–7284.
- [9] XU J L, CHEN C. The research of materials microstructure analysis [J]. Acta Metrologica Sinica, 2004, 4: 369–373. (in Chinese)
- [10] MIN Dong, SHEN Jun, LAI Shi-qiang, CHEN Jie. Effect of heat input on the microstructure and mechanical properties of tungsten inert gas arc butt-welded AZ61 magnesium alloy plates [J]. Materials Characterization, 2009, 60(12): 1583–1590.
- [11] HEIPLE C R, ROPER J R. Effect of selenium on GTAW fusion zone geometry [J]. Welding Journal, 1981, 60(8): 143.
- [12] HEIPLE C R, ROPER J R. Mechanism for minor element effect on GTA fusion zone geometry [J]. Welding Journal, 1982, 61(4): 97–102.
- [13] ZHANG Z D, LIU L M, SHEN Y, WANG L. Mechanical properties and microstructures of a magnesium alloy gas tungsten arc welded with a cadmium chloride flux [J]. Materials Characterization, 2008, 59(1): 40–46.
- [14] SHEN Jun, WANG Lin-zhi, PENG Dong, WANG Dan. Effects of CaF₂ coating on the microstructures and mechanical properties of tungsten inert gas welded AZ31 magnesium alloy joints [J]. Metallurgical and Materials Transactions A, 2012, 43(11): 4397–4405.
- [15] LIANG G, YUAN S. Study on the temperature measurement of AZ31B magnesium alloy in gas tungsten arc welding [J]. Materials Letters, 2008, 62(15): 2282–2284.
- [16] CAO X, JAHAZI M. Effect of welding speed on the quality of friction stir welded butt joints of a magnesium alloy [J]. Materials & Design, 2009, 30(6): 2033–2042.
- [17] MERIÇ C, ATIK E, ENGEZ T. Experimental microhardness for AA 1030, Cu, CuSn7, CuZn30 and 6114 alloys and a correlation with the Hall–Petch relation [J]. Materials Research Bulletin, 1999, 34(12): 2043–2052.
- [18] XUNHONG W, KUAISHE W. Microstructure and properties of friction stir butt-welded AZ31 magnesium alloy [J]. Materials Science and Engineering A, 2006, 431(1): 114–117.

焊接电流对涂覆 TiO₂ 活性剂 AZ31 镁合金 TIG 焊的影响

沈 骏, 翟大军, 刘 凯, 曹中明

重庆大学 材料科学与工程学院, 重庆 400044

摘 要: 研究焊接电流对涂覆 TiO₂ 活性剂 AZ31 镁合金板材活性钨极氩弧焊(A-TIG)焊接接头的宏观形貌、微观结构和力学性能的影响。实验结果表明, 随着焊接电流的增加, 焊缝的熔深和熔宽比增加, 涂覆 TiO₂ 的焊缝表面形貌逐渐恶化; 焊缝中 α -Mg 晶粒尺寸增加, 颗粒状 β -Mg₁₇Al₁₂ 数量增多。与普通的 TIG 焊相比, A-TIG 焊缝熔深明显增加并且晶粒尺寸粗化。当焊接电流小于 130 A 时, 涂覆 TiO₂ 焊接接头的极限抗拉强度值随着焊接电流的增加而增加, 当焊接电流超过 130 A 时其抗拉强度值开始下降; 焊缝热影响区和熔合区的平均显微硬度随着焊接电流的增加逐渐降低。

关键词: AZ31 镁合金; A-TIG 焊接; 焊接电流; TiO₂ 活性剂

(Edited by Sai-qian YUAN)